CHEMISTRY OF MATERIALS

Article

pubs.acs.org/cm

Surface Functionalization of Zinc Oxide Nanoparticles: An Investigation in the Aerosol State

Chi-Tung Chiang[†] and Jeffrey T. Roberts*[,†]

Department of Chemistry, Purdue University, 560 Oval Drive, West Lafayette, Indiana 47907, United States

Department of Chemistry, University of Minnesota, 207 Pleasant Street SE, Minneapolis, Minnesota 55455, United States

ABSTRACT: The interactions of the simple amine functional groups with the surfaces of ZnO aerosol nanoparticles have been investigated. The ZnO particles were synthesized from the metal−organic precursor methylzinc isopropoxide {$[CH_3ZnOCH(CH_3)_2]_4$, MZI}. Solid MZI was evaporated at 85−120 °C, and then swept by an inert carrier gas at atmospheric pressure through a tube furnace operating at 300−900 °C. Thermal decomposition of MZI led to the formation of stoichiometric ZnO nanoparticles of mobility diameter 3−50 nm. The size, structure, and composition of synthesized particles were characterized by differential mobility analysis (DMA), X-ray diffraction (XRD), transmission electron microscopy (TEM), and Fourier transform IR spectroscopy (FTIR). The aerosolized ZnO nanoparticles were reacted with two gas-phase organic species: 1-butylamine and 1-hexylamine. Uptake was monitored by tandem differential mobility analysis (T-DMA). These results represent the first work on surface functionalization of ZnO nanoparticles in the aerosol state. They establish a new approach for manipulating quantum dot materials in the aerosol state.

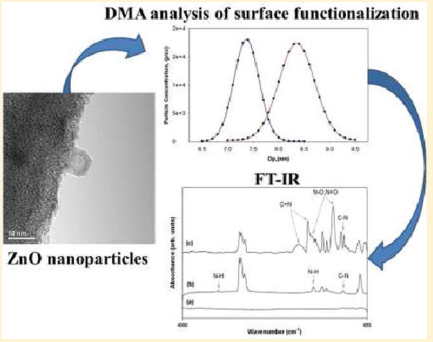

KEYWORDS: *ZnO nanoparticles, aerosol, differential mobility analyzer, surface functionalization, IR*

INTRODUCTION

ZnO is a versatile semiconductor with high-excitation binding energy (60 meV) and a wide band gap (3.37 eV) at room temperature.[1,2] In nanoparticle form, ZnO has been considered as a promising material in solar cell,[3,4] gas sensor,[5] photocatalyst,[6] and light-emitting diode applications.[7,8] Many techniques have been developed to synthesize ZnO nanoparticles, including mechanical milling,[9] aqueous precipitation,[10] pulsed laser ablation,[11] electrochemical synthesis,[12] sol−gel synthesis,[13] and mechanochemical processing.[14] Within the growing literature on ZnO nanoparticles, the subject of surface functionalization has attracted increasing attention since the addition of functional groups on the particle surface can alter the properties of particles.[15−18] For example, in biological systems the surface layer of nanoparticles can play a multifunctional role: a linker to the surrounding environment, a protection layer, the focus of antigen detection and most importantly biocompatibility.[19] To the best of our knowledge, previous attempts to functionalize ZnO nanoparticle surfaces have involved wet chemical methods. This has numerous disadvantages, for instance, the existence of residual solvent post-synthesis and the difficulty of devising and continuous processing methods.

One of the alternative routes to achieve the surface functionalization of nanoparticles is the aerosol state process. Recent developments of differential mobility analysis (DMA)[20] allow the particle size distribution in the aerosol stream be precisely analyzed by their electrical mobility in real time. DMA can operate either in fixed mode for size-selection or scan mode for size distribution measurements. With a reliable particle generation method, the aerosol state process can be operated continuously. Changes in size of nanoparticles provide the most evident results corresponding to all reactions occurred. Many DMA measurements have been carried out to identify a variety of chemical and physical phenomena, such as oxidation,[21,22] adsorption,[23] desorption,[24] dissolution,[25] and nanoparticle agglomeration.[26]

A gas-phase synthesis was recently reported by Polarz et al.,[27] providing an alternative route to ZnO nanoparticles. The method involves the evaporation and decomposition of the metal−organic precursor methylzinc isopropoxide {$[CH_3-ZnO-CH(CH_3)_2]_4$, MZI}. The synthesis of the precursor can be expressed by eq 1.

$$4Zn(CH_3)_2 + 4(CH_3)_2CHOH \rightarrow [CH_3 - ZnO - CH(CH_3)_2]_4(MZI) + 4CH_4 \quad (1)$$

The formation of ZnO nanoparticles results from the decomposition of MZI vapor in the presence of molecular oxygen at high temperatures (>300 °C).

Here, we report a new approach to the surface functionalization of ZnO nanoparticles by reacting particles with organic monolayer precursors in the gas/aerosol state. The ZnO

Received: August 3, 2011
Revised: November 1, 2011
Published: November 3, 2011

nanoparticles were synthesized from the metal−organic precursor, MZI. Various experimental conditions were investigated to optimize the particle size and quality before functionalization. Organic vapor was introduced into a ZnO nanoparticles stream. The aerosolized ZnO nanoparticles were reacted with two gas-phase organic precursors, including 1-butylamine and 1-hexylamine. The size, structure, and composition of synthesized particles were characterized by DMA, X-ray diffraction (XRD), transmission electron microscopy (TEM), and Fourier transform IR spectroscopy (FT-IR). The present work represents the first investigation in surface functionalization of ZnO nanoparticles in the aerosol state.

EXPERIMENTAL SECTION

Synthesis of MZI Precursor. The precursor was synthesized on the basis of a literature method.[27] Synthesis and handlings were conducted using standard glovebox and Schlenck techniques. All chemicals were obtained from Aldrich. Diethyl ether and benzene-d^8 were distilled over CaH_2 under N_2. Isopropanol was dried with 3 A molecular sieves under N_2. In a typical run, a commercial 2 M solution of $Zn(CH_3)_2$ (100 mmol) in 50 mL of toluene was transferred into a 500 mL, three-necked flask, to which 200 mL of diethyl ether was added. The solution was cooled at −78 °C, and isopropanol (7.66 mL, 100 mmol) was added via a syringe. After the solution was stirred at −78 °C for 0.5 h, it was warmed to room temperature and stirred overnight. The solvents were then partially removed under vacuum to afford a solution of ca. 80 mL. Trace insoluble materials were removed by filtration, to afford a colorless, clear solution. The solution was concentrated to ca. 40 mL and stored at −20 °C. After several days, a colorless, crystalline solid (MZI) was precipitated and isolated (12.1 g, 87% yield). The product was identified by comparing its ^1H and ^{13}C NMR spectra to the published MZI data.

Methods. Experiments were carried out using house-built aerosol flow tubes at atmospheric pressure (Figure 1). Solid

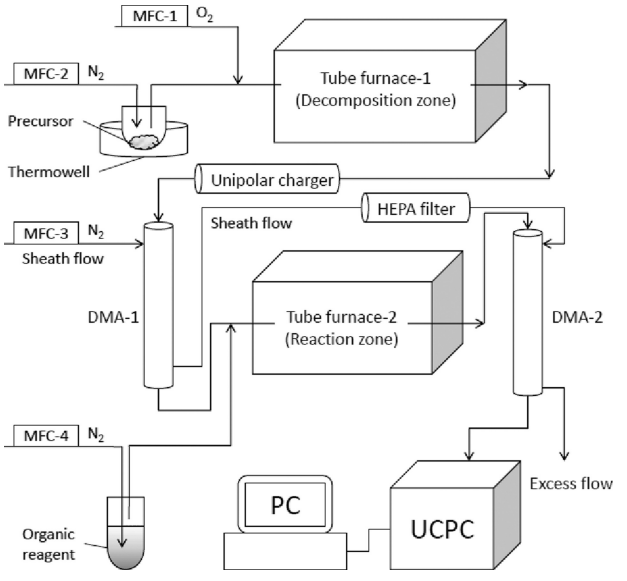

Figure 1. Schematic drawing of experimental apparatus.

MZI was placed in the precursor vessel, and was driven into the gas phase by heating the thermowell to 85−120 °C. Aerosolized ZnO nanoparticles were synthesized by flowing N_2/O_2 mixtures across the precursor vessel and then through the decomposition tube furnace. The aerosol stream containing newly formed ZnO nanoparticles was passed through a bipolar diffusion charger and then through a differential mobility analyzer, DMA-1 (nanoDMA 3085, TSI Inc., Shoreview, MN). DMA-1 was adjusted to transmit only negatively charged particles. The resulting particles were then directly scanned in conjunction with an ultrafine condensation particle counter (UCPC 3776, TSI Inc., Shoreview, MN) to determine the size distribution and concentration of particles in the aerosol. Table 1

Table 1. Experimental Conditions

component	settings	
MFC-1 (O_2)	0−500	sccm
MFC-2 (N_2)	1000−1500	sccm
MFC-3 (N_2)	15000	sccm
MFC-4 (N_2)	0−200	sccm
tube furnace-1 (T_D)	RT-900	°C
tube furnace-2 (T_R)	RT-500	°C
thermowell	85−120	°C
UCPC intake flow rate	1500	sccm
decomposition zone length	30.5	cm
reaction zone length	30.5	cm

lists typical experimental conditions. Mass flow controllers (MFC, Model 1179, MKS Instruments, Andover, MA) were used to supply constant operating flow rates. The combined N_2 and O_2 flow was set to 1500 sccm in order to accommodate the intake flow of particle counter. The optimal condition for particle formation was obtained at 1200 sccm of N_2 flow and 300 sccm of O_2 flow. In the surface functionalization experiments, DMA-1 was fixed to transmit 8.0 nm particles to the reaction zone, and the organic reagents were added immediately after the mobility-selected stream. Organic reagent vapor was introduced into the reaction zone by passing N_2 of known flow rate through a bubbler containing the liquid state reagent. Two organic reagents were chosen as surface modification agents: 1-butylamine and 1-hexylamine. Temperatures of the decomposition zone and the reaction zone both could be set between room temperature and 1200 °C. All tubes used in this work were stainless steel and were capable of being heated up to 1000 °C. The estimated particle residence times in the decomposition (τ_1) and reaction zone (τ_2) were varied by the diameter the tubes used: τ_1 = 0.4 s (6 mm diameter tube) and τ_2 = 1.6 s (12 mm diameter tube). Changes in mobility diameter that resulted from surface functionalization were measured using tandem differential mobility analysis (T-DMA) that DMA-2 and the UCPC was used to scan the selected particles after the reaction zone. At least three separate DMA or T-DMA scans were obtained for each set of conditions. Two types of sample collection were used, including an electrostatic sampler in the range of 1.0−5.0 kV and inertial impaction onto stainless steel meshes and corning glasses. TEM images were obtained using a Tecnai T12 microscope (FEI Company, Hilsboro, OR) at an accelerating voltage of 120 kV. XRD patterns of particles were analyzed by a microdiffractometer (Bruker-AXS, Madison, WI) with 2.2 kW sealed Cu X-ray Source. Diffuse reflectance Fourier transform infrared spectroscopy (DRIFTS) was used to detect the functional group of collected particle samples. IR spectra of collected particles were obtained using Nicolet Magna-IR 750 spectrometer equipped with a diffuse reflectance accessory from Harrick Seagull.

dx.doi.org/10.1021/cm202278z|Chem. Mater. 2011, 23, 5237−5242

RESULTS AND DISCUSSION

Characteristics of Synthesized ZnO Nanoparticles.

Figure 2 shows representative mobility diameter distribution of

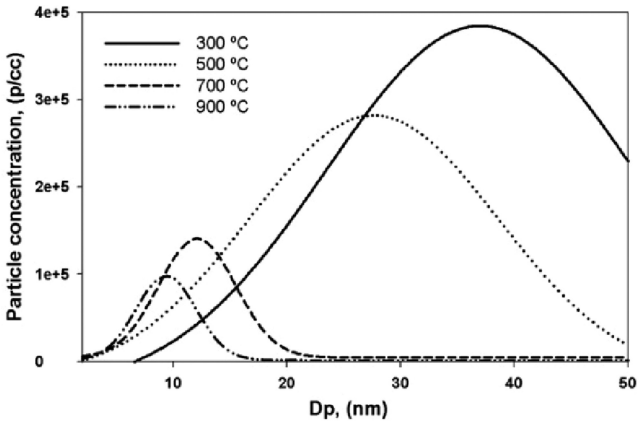

Figure 2. Size distributions of prepared ZnO nanoparticles as a function of the decomposition zone temperature (T_D) acquired at N_2, 1200 sccm; and O_2, 300 sccm.

nanoparticles prepared at different decomposition zone temperatures (T_D). This result shows that the size distributions of particles prepared by MZI decomposition depend strongly on temperature. As the furnace temperature is increased, the peak particle size shifts down in size, and the total measured particle concentration decreases substantially, especially between T_D = 700 and 900 °C. It is noteworthy that the increase in peak size is also associated with an increase in residence time in the hot zone of the reactor. Figure 3 displays

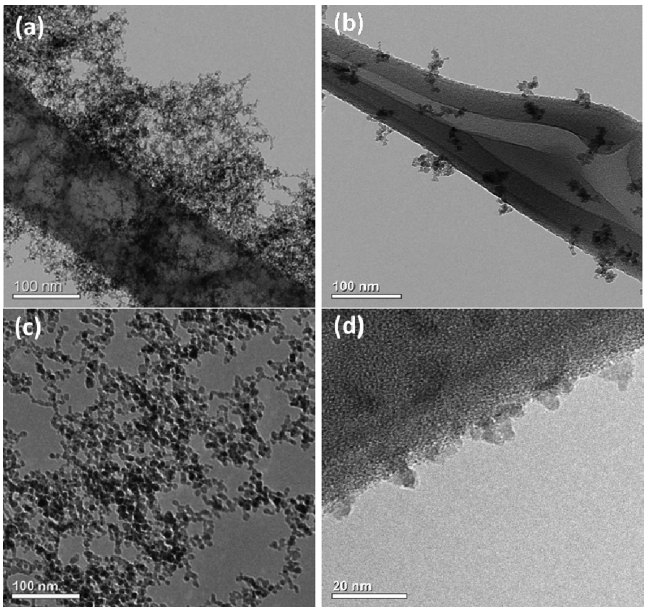

Figure 3. TEM images of prepared nanoparticles at decomposition zone temperature at (a) 300 and (c) 900 °C, and mobility-selected (b) 20 nm nanoparticles at 300 °C and (d) 10 nm nanoparticles at 900 °C .

representative transmission electron microcopy images of as-prepared and mobility-selected particles prepared at T_D = 300 and 900 °C. As-prepared particle samples were deposited on TEM grids by inertial impaction in the downstream of decomposition zone. For mobility-selected particles, samples were collected using the electrostatic sampler. Images of as-prepared particle samples both show that many particles are aggregates, but particles prepared at 900 °C appears to be larger and more disperse. Images of mobility-selected 20 nm particles prepared at 300 °C show that each selected particle is a cluster of several smaller particles.

The chemical composition of prepared nanoparticles was investigated by Fourier transform infrared spectroscopy (FT-IR), as shown in Figure 4. The principle IR stretching band of micro-

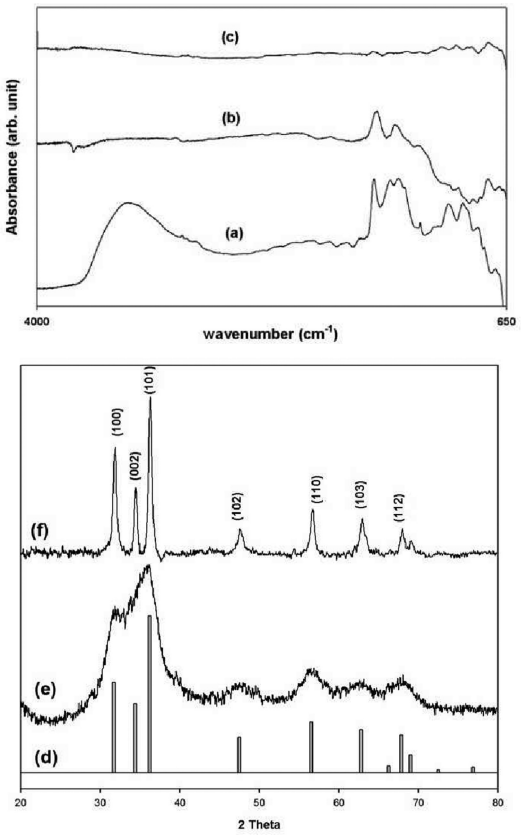

Figure 4. FT-IR spectra of ZnO nanoparticles prepared at decomposition zone temperature T_D = (a) 300, (b) 700, and (c) 900 °C. XRD patterns of (d) standard ZnO, and ZnO nanoparticles prepared at T_D = (e) 300 and (f) 900 °C.

crystalline ZnO is at ca. 500 cm^{-1},[28] which is below the range of the detector for the FT-IR spectrometer employed in these experiments. However, FT-IR can identify organic functional groups. At T_D = 300 °C, the IR spectrum of freshly generated particles are dominated by peaks at 3350, 1590, 1450, 1060, and 950 cm^{-1}, features that are associated with hydroxyl, bidentate carbonate group and various hydrocarbon stretching vibrations, respectively.[27,29] These peaks suggest incomplete decomposition of MZI, resulting in organic groups bound in or on the ZnO particles. At T_D = 700 °C, only peaks at 1590 and 1450 cm^{-1} are present in the spectrum, suggesting more complete decomposition at higher temperatures. However, spectra recorded for particles collected at T_D = 900 °C show virtually no peaks in the infrared, consistent with complete decomposition to form ZnO nanoparticles without organic adsorbates. X-ray diffraction (XRD) was performed in order to confirm the crystalline structure of the

dx.doi.org/10.1021/cm202278z|Chem. Mater. 2011, 23, 5237–5242

prepare ZnO nanoparticles. XRD patterns of standard ZnO and two samples obtained at T_D = 300 and 900 °C (see Figure 4) show that the higher T_D is the key factor to form stoichiometric ZnO nanoparticles. The XRD pattern obtained at T_D = 900 °C is in good agreement with the standard ZnO, which is generally assigned to the hexagonal wurtzite structure in space group P63mc with lattice constants a = 3.250 and c = 5.207 Å.[30]

At lower temperatures (T_D = 300 °C), both FT-IR and XRD result provide direct evidence that the decomposition process is incomplete. At high temperature (T_D = 900 °C), the resulting aerosol stream contains adsorbate-free, crystalline, and monodisperse ZnO nanoparticles, which has reached the condition required as a particle source for surface functionalization.

Surface Functionalization of Mobility-Selected 8.0 nm Particles. On the basis of the characteristics of prepared ZnO nanoparticles and considerations of particle concentration and detection limit of the apparatus, surface functionalization experiments were conducted on mobility-selected 8.0 nm particles prepared at T_D = 900 °C. Representative TEM images of mobility-selected 8.0 nm ZnO particles collected on the TEM grid are shown in Figure 5. The images are qualitatively in agreement with the selected mobility diameter. Changes in mobility diameter of selected 8.0 nm particles before and after the reaction zone were monitored by tandem differential mobility analysis (T-DMA).[31] This technique is capable of measuring monolayer uptake on particles through changes in peak particle mobility diameter.[22−24] Representative particle size distributions without amine flow (Figure 5b) show that the peak diameter is 8.4 nm at the reaction zone temperature (T_R) = 25 °C. The increase in particle size can be explained by the possibility of impurity adsorption, such as water vapor, in the reaction zone, or structural relaxation due to ambient temperature. However, both peak diameter and particle concentration decrease as T_R increases, with peak mobility diameter shrinking to 7.0 nm at 400 °C. We interpret this as evidence either for thermally induced particle restructuring or for desorption of adsorbed material.

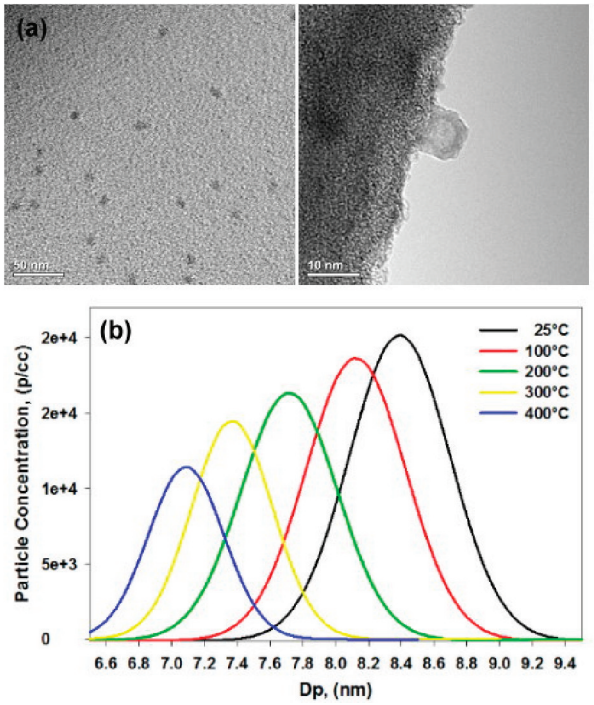

Figure 5. TEM images of mobility-selected 8.0 nm ZnO nanoparticles. (a) Left: a low-magnification image. Right: a high-magnification image. The dark region is the lacey carbon support on TEM grid. (b) Size distributions of mobility-selected 8.0 nm ZnO nanoparticles as a function of the reaction zone temperature (T_R).

Figure 6a shows representative T-DMA scans of 8.0 nm mobility-selected particles that passed through the reaction zone at 300 °C, with and without 1-hexylamine exposure. Under this set of conditions, the peak of particle diameter in the distribution is quantified by the increase from 7.4 to 8.4 nm after reaction with 1-hexylamine. The broader full width at half-maximum (fwhm) in the size distribution of 1-hexylamine exposed particles may be an indication of multiple attachment of amine molecules, which could affect the distribution width. Figure 6b is the plot of Dp, the peak mobility diameter, vs furnace settings from T_R = room temperature (RT) to 400 °C with plots at different flow rate of nitrogen through the 1-hexylamine bubbler. The peak mobility diameter after the reaction zone shows that the particles size remains roughly at 8.5 ± 0.1 nm and the maximum is at 8.9 nm. Compared to the plot of uncoated ZnO nanoparticles, the change in peak diameter increases as T_R rises, and reaches a maximum

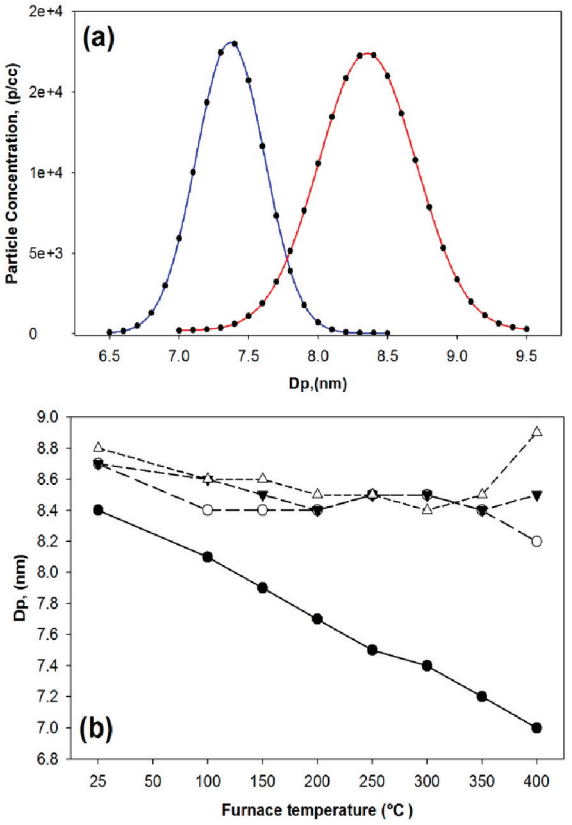

Figure 6. (a) T-DMA scans of 8.0 nm mobility-selected particles without (blue line) and with (red lines) 1-hexylamine exposure. The reaction zone temperature was at T_R = 300 °C with 50 sccm N_2 carrier gas flow. (b) Peak mobility diameter (Dp, nm) plotted against the reaction zone temperature (T_R). The N_2 carrier gas flow rates in the 1-hexylamine vessel were 12 sccm (○), 25 sccm (▼), and 50 sccm (Δ). The lowest line is data of the uncoated ZnO nanoparticles (●) taken from Figure 5b.

dx.doi.org/10.1021/cm202278z|Chem. Mater. 2011, 23, 5237−5242

at T_R = 400 °C. It appears that the N_2 flow rate is not a major factor during the processes, suggesting a very reactive process between 1-hexylamine molecules and particle surface that the amine adsorption could take place even with trace amount of 1-hexylamine vapor presented at reaction zone. The most probable particle diameter difference (ΔDp) between coated and uncoated particles at T_R = 400 °C is at 1.5 nm, which implies an average 0.75 nm layer on particles and such thickness is roughly equal to the length of 1-hexylamine molecule.

In the case of 1-butylamine, ΔD_p was 1.2 nm at T_R = 400 °C, also suggesting a nearly saturated layer of 1-butylamine on ZnO after interaction. At that temperature, the most probable peak particle size was 8.0 ± 0.1 nm, with size change only weakly dependent on the N_2 flow rate. Note that saturated particles were unable to be observed above T_R = 400 °C because the resulting particle concentration diminished significantly.

Figure 7 shows IR spectra of neat 1-butylamine, and of coated and uncoated ZnO nanoparticles. The neat 1-butylamine spectrum was obtained by directly dropping 0.5 mL of liquid onto a mesh and the coated sample was collected at T_R =300 °C with1-butylamine exposure. No peak on a spectrum of uncoated particles implies the adsorbate-free ZnO particles. The spectrum of neat 1-butylamine is dominated by the C−H (2962, 2932, 2872, 1462, and 1382 cm^{-1}), N−H (3346 and 1627 cm^{-1}), C−N (1086 cm^{-1}), and C−C skeleton (781 cm^{-1}) stretching bands, which are assigned by published IR database.[29] For coated particles, the spectra exhibits some similarities with the neat 1-butylamine spectrum in the C−H, C−N, and C−C stretching bands. However, there are new features as well. The broad band ranging between 1700 and 2000 cm^{-1} is assigned to C═N stretching vibration, and peaks at 1652 and 1265 cm^{-1} are attributed to N−O and N═O stretching regions.[29] The details of the interaction between Zn moiety and amines in the spectrum could not be determined due to the lack of known Zn related stretching bands and the used spectral range. However, the spectra provide strong evidence to support the T-DMA results that the increase in mobility diameter is due to amine adsorption onto the surfaces of ZnO particles. That is, the interaction between the oxygen moiety of ZnO nanoparticles and long pair electrons of amine can lead to the formation of N−O and N═O nitroso bonds along with dehydrogenation within the amine skeleton (loss of N−H bonds). The proposed reaction for 1-butylamine adsorbed on the surface of ZnO nanoparticles is shown in Scheme 1. Note that the surface of ZnO nanoparticles has been functionalized with amine molecules, but the adsorbed layer is believed to be only partially saturated on the surface of particles because only limited evidence of fully saturated particles was obtained from T-DMA experiment.

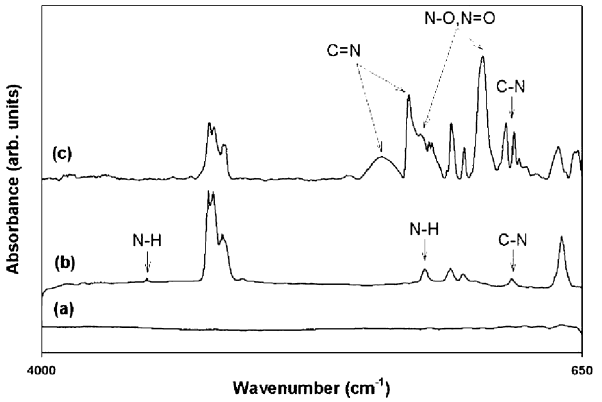

Figure 7. IR spectra of (a) uncoated ZnO nanoparticles, (b) neat 1-butylamine, and (c) ZnO nanoparticles coated with 1-butylamine.

Scheme 1. Proposed Reactions between ZnO Nanoparticles and Butylamine Molecules

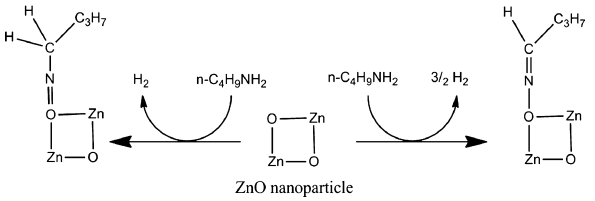

CONCLUSIONS

In summary, this is the first investigation to functionalize the surfaces of ZnO nanoparticles in the aerosol state. Aerosolized ZnO nanoparticles were synthesized by flowing nitrogen gas through the heated particle precursor MZI and further conditioning with oxygen flow in the decomposition zone. Particles with good crystalline and chemical qualities prepared at T_D = 900 °C served as the source particles for the surface functionalization. Mobility-selected 8.0 nm particles were reacted with amines in the gas phase in a temperature-controlled reaction zone. As the reaction zone temperature increases, the diameter of neat mobility-selected particle decreases but maintains nearly the same particle size with the amine exposure. The bonding between particles and amines were characterized by FT-IR to confirm the presence of an adsorbed layer on the surface of ZnO nanoparticles. Given the properties and size of particles studied in this work, the ZnO nanoparticles prepared here can be considered as a type of quantum dots (QDs).[32] Further investigation is required to identify the change in their quantum confinement effect before and after the surface functionalization. However, the present work provides a new approach for exploring the possibility to process the surface of quantum dot materials in the aerosol state.

AUTHOR INFORMATION

Corresponding Author

*E-mail: jtrob@purdue.edu.

Notes

†The authors relocated from University of Minnesota to Purdue University in August 2009. The present work was conducted at both institutions.

ACKNOWLEDGMENTS

Parts of this work were carried out in the Institute of Technology Characterization Facility, University of Minnesota, a member of the NSF-funded Material Research Facilities Network (www.mrfn.org). The authors extend thanks to Dr. Bing Luo for his assistance and comments in synthesizing the MZI precursor.

REFERENCES

(1) Wong, E. M.; Searson, P. C. *Appl. Phys. Lett.* **1999**, *74*, 2939.
(2) Kong, X. Y.; Ding, Y.; Yang, R. S.; Wang, Z. L. *Science* **2004**, *303*, 1348.

(3) O'Regan, B.; Grätzel, M. A. *Nature* **1991**, *353*, 737.
(4) Yoshida, T.; Terada, K.; Schlettwein, D.; Oekermann, T.; Sugiura, T.; Minoura, H. *Adv. Mater.* **2000**, *12*, 1214.
(5) Kind, H.; Yan, H.; Messer, B.; Law, M.; Yang, P. *Adv. Mater.* **2002**, *14*, 158.
(6) Jang, E. S.; Won, J.-H.; Hwang, S.-J.; Choy, J.-H. *Adv. Mater.* **2006**, *18*, 3309.
(7) Colvin, V. L.; Schlamp, M. C.; Alivisatos, A. P. *Nature* **1994**, *370*, 354.
(8) Look, D. C.; Reynolds, D. C.; Litton, C. W.; Jones, R. L.; Eason, D. B.; Cantwell, G. *Appl. Phys. Lett.* **2002**, *81*, 1830.
(9) Damonte, L. C.; Mendoza Zélis, L. A.; Marí Soucase, B.; Hernández Fenollosa, M. A. *Powder Technol.* **2004**, *148*, 15.
(10) Li, M.; Hari-Bala, Lv, X.; Ma, X.; Sun, F.; Tang, L.; Wang, Z. *Mater. Lett.* **2007**, *61*, 690.
(11) He, C.; Sasaki, T.; Usui, H.; Shimizu, Y.; Koshizaki, N. *J. Photochem. Photobiol. A* **2007**, *191*, 66.
(12) Starowicz, M.; Stypuła, B. *Eur. J. Inorg. Chem.* **2008**, *6*, 869.
(13) Chu, S. Y.; Yan, T. M.; Chen, S. L. *J. Mater. Sci. Lett.* **2000**, *19*, 349.
(14) Moballegh, A.; Shahverdi, H. R.; Aghababazadeh, R.; Mirhabibi, A. R. *Surf. Sci.* **2007**, *601*, 2850.
(15) Wu, Y. L.; Tok, A. I. Y.; Boey, F. Y. C.; Zeng, X. T.; Zhang, X. H. *Appl. Surf. Sci.* **2007**, *253*, 5473.
(16) Tang, E.; Cheng, C.; Ma, X.; Pang, X.; Zhao, Q. *Appl. Surf. Sci.* **2006**, *252*, 5227.
(17) Wu, Y. L.; Lim, C. S.; Fu, S.; Tok, A. I. Y.; Lau, H. M.; Boey, F. Y. C.; Zeng, X. T. *Nanotechnology* **2007**, *18*, 215604.
(18) Khrenov, V.; Klapper, M.; Koch, M.; Müllen, K. *Macromol. Chem. Phys.* **2005**, *206*, 95.
(19) Salata, O. V. *J. Nanobiotechnol.* **2004**, *2*, 3.
(20) Chen, D.-R.; Pui, D. Y. H.; Hummes, D.; Fissan, H.; Quant, F. R.; Sem, G. J. *J. Aerosol Sci.* **1998**, *29* (5), 497.
(21) Higgins, K. J.; Jung, H.; Kittelson, D. B.; Roberts, J. T.; Zachariah, M. R. *J. Phys. Chem. A* **2002**, *106* (1), 96.
(22) Holm, J.; Roberts, J. T. *Langmuir* **2007**, *23*, 11217.
(23) Liao, Y.-C.; Roberts, J. T. *J. Am. Chem. Soc.* **2006**, *128*, 9061.
(24) Holm, J.; Roberts, J. T. *J. Am. Chem .Soc.* **2007**, *129*, 2496.
(25) Elzey, S.; Grassian, V. H. J. *Langmuir* **2010**, *26*, 12505.
(26) Park, K.; Kittelson, D. B.; Zachariah, M. R.; McMurry, P. H. *J. Nanopart. Res.* **2004**, *6*, 267.
(27) Polarz, S.; Roy, A.; Merz, M.; Halm, S.; Schröder, D.; Schneider, L.; Bacher, G.; Kruis, F. E.; Driess, M. *Small* **2005**, *1* (5), 540.
(28) Hlaing, Oo, W. M.; McCluskey, M. D.; Huso, J.; Bergman, L. *J. Appl. Phys.* **2007**, *102*, 043529.
(29) Stein, S. E. IR and Mass Spectra. In *NIST Chemistry WebBook*; Mallard, W. G., Linstrom, P. J., Eds.; NIST Standard Reference Database Number 69; National Institute of Standards and Technology: Gaithersburg, MD, 2000; http://webbook.nist.gov.
(30) Kisi, E. H.; Elcombe, M. M. *Acta Crystallogr., Sect. C* **1989**, *45*, 1867.
(31) Rader, D. J.; McMurry, P. H. *J. Aerosol Sci.* **1986**, *17*, 771.
(32) Yang, S. J.; Park, C. R. *Nanotechnology* **2008**, *19*, 035609.